Available online at scholarcommons.usf.edu/ijs

International Journal of Speleology

Official Journal of Union Internationale de Spéléologie

Response of Botovskaya Cave to local and regional environmental dynamics

Jade Margerum [1*], Oksana Gutareva [2], Franziska A. Lechleitner [3], Maria Box [1], Stuart Umbo [1,4], Anton Vaks [5], Hanno Meyer [6], Aleksandr Kononov [2,7], Alexander Osintsev[8], Dimitri Sokol'nikov[8], Norbert Marwan [9], Ola Kwiecien [1], and Sebastian F.M. Breitenbach [1]

[1]School of Geography and Natural Sciences, Northumbria University, Newcastle-Upon-Tyne, NE1 8ST, UK
[2]Institute of the Earth's Crust, Russian Academy of Sciences, Siberian Branch, Irkutsk, 664033, Russia
[3]Department of Chemistry, Biochemistry and Pharmaceutical Sciences & Oeschger Centre for Climate Change Research, Universität Bern, Freiestrasse 3, 3012 Bern, Switzerland
[4]Department of Natural Sciences, Manchester Metropolitan University, Manchester, United Kingdom
[5]Geological Survey of Israel, 32 Yeshayahu Leibowitz Street, 9692100 Jerusalem, Israel
[6]Alfred Wegener Institute Helmholtz Center for Polar and Marine Research, Polar Terrestrial Environmental Systems Section, Telegrafenberg A45, 14473 Potsdam, Germany
[7]Irkutsk National Research Technical University, Irkutsk, 664074, Russia
[8]Speleoclub Arabika, St. Mamina-Sibiryaka 6a, 664058 Irkutsk, Russia
[9]Potsdam Institute for Climate Impact Research, Potsdam, Germany

Abstract: Speleothems from caves in near-permafrost regions can provide unique insights into the climatic history of temperature-sensitive environments. These regions are often remote and only seasonally accessible, which makes cave monitoring – a requirement for speleothem-based proxy interpretation – challenging. We document ventilation, the infiltration regime, and the isotopic composition of dripwater in Botovskaya Cave in southern Siberia, a host to speleothems previously used to reconstruct Quaternary permafrost dynamics in continental Eurasia. We explore surface and cave temperature records, cave air CO_2 concentration data and stable isotopes in precipitation and dripwater and evaluate infiltration conditions and the sensitivity of speleothems to regional atmospheric dynamics. Locations further into the cave are thermally more stable (T = 1.8 – 2.5 ± 0.1°C) than sites closer to the entrances which show inter-seasonal temperature variability of ca. 4°C. Cave CO_2 concentration is highest during summer when the cave acts like a cold trap and cave air becomes stagnant and in winter when frozen ground and epikarst and entrances closed by snow subdue ventilation. Accordingly, sub-horizontal Botovskaya Cave ventilates via vertical joints and the entrances during spring whenever cave air is warmer than the surface air. Dripwater isotopic composition ($\delta^{18}O$ and $\delta^{2}H$) generally reflects the mean isotopic composition of precipitation, but $\delta^{18}O$ decreases with distance from the entrances, and in the deeper sections of the cave reflects the mean (multi)annual isotopic composition in precipitation, likely due to an increasing contribution of snowmelt to total infiltration. Slope aspect and vegetation density above the cave section determine the proportion of received seasonal precipitation. On local scale our results provide insights into the environmental processes that govern the microclimate in Botovskaya Cave and facilitate robust interpretation of future speleothem-based proxy reconstructions. On the pan-regional scale we propose a potential mechanism responsible for suboptimal reproducibility of stalagmite records from the same cave.

Keywords: Siberia, cave monitoring, dripwater isotopes, cave ventilation, stalagmite growth

Received 23 November 2025; Revised 20 February 2026; Accepted 28 February 2026

Citation: Margerum, J., Gutareva, O., Lechleitner, F.A., Box, M., Umbo, S., Vaks, A., Meyer, H., Kononov, A., Osintsev A., Sokol'nikov D., Marwan, N., Kwiecien O., Breitenbach S.F.M., 2026. Response of Botovskaya Cave to local and regional environmental dynamics. International Journal of Speleology, 54(3), ijs2587. https://doi.org/10.5038/1827-806X.ijs2587

INTRODUCTION

Caves located on the fringe of permafrost regions are subject to extreme environmental conditions and are often found in remote and sometimes inaccessible areas. In the mid-high latitude continental interior of Eurasia, extreme surface air temperature seasonality supports long, freezing winters with temperatures

*jade.margerum@northumbria.ac.uk

plummeting to ca. -50°C, and short mild summers with maximum temperatures of ca. 30°C. The effects of such harsh and seasonally variable conditions can produce challenges when interpreting speleothem proxy records (cave carbonate deposits responsive to climatic changes) originating from the sub-permafrost region. Permafrost can limit infiltration into caves and prevent speleothem growth, such as during glacial intervals (Vaks et al., 2013, 2020, 2025; Lechleitner et al., 2020), on the centennial – decadal scale (i.e., Little Ice Age), or annual scale via freezing during winter months. The effects on seasonal infiltration into caves can produce proxy bias towards summer months when infiltration is not limited by frozen grounds, and can affect the interannual variability, composition, and rate of dripwaters which determine speleothem morphology, size, and shape (Frisia et al., 2019).

Characterization of cave environments is fundamental for interpretation of speleothem proxies, which are governed by both outside environmental and in-cave microclimatic conditions, however monitoring of caves close to permafrost regions has numerous challenges. Many of these caves suffer the mechanistic destruction of freeze-thaw cycling and limit research to caves with good structural integrity. Sub-zero surface temperatures can negatively affect monitoring equipment during winter periods (loss of battery life if kept in low temperatures, performance and accuracy issues) and extreme temperature seasonality can limit the expedition window, making frequent visits to a study site impossible and prolonging and/or delaying data collection. As a result, monitoring of caves near permafrost conditions are underrepresented in literature.

Environmental proxies like stable oxygen and carbon isotopes, biomarkers, or element concentrations are measured in speleothems because they react to environmental dynamics at the surface (Baldini et al., 2021; Wong & Breecker, 2015). However, these proxies are often influenced by multiple environmental processes, and without detailed microclimatic monitoring provide only qualitative information. Recent studies employing speleothems have explored the permafrost history of Siberia and teleconnections to Arctic sea ice conditions during the Quaternary and Miocene (Vaks et al., 2013, 2020, 2025), mid-Holocene hydroclimate (Columbu et al., 2023), and fire and vegetation dynamics of the Holocene and Last Interglacial (Margerum et al., 2025). Many of the speleothems utilized for the study of the Quaternary and Miocene in southern Siberia originate from Botovskaya Cave (Pacton et al., 2013; Vaks et al., 2013, 2020, 2025; Margerum et al., 2025), just outside of the permafrost zone.

Here, we compliment these studies with over a decade of monitoring data from Botovskaya Cave, including surface and cave air temperature, relative humidity and CO_2 in the cave, and dripwater isotope ($\delta^{18}O$ and $\delta^{2}H$) signals. Our multi-parameter monitoring offers new insights into the ventilation dynamics and moisture budget of Botovskaya Cave that help elucidate the sensitivity of speleothems against environmental changes in continental Eurasia. We characterize key surface and subsurface parameters, including temperature and precipitation regimes, to develop a comprehensive understanding of the mechanisms that influence the deposition of and proxy dynamics in speleothems in Botovskaya Cave. We explore the effects of cave ventilation and seasonality on the formation of speleothems and implications to proxy systems.

CAVE SETTING, REGIONAL CLIMATE AND ENVIRONMENT

Botovskaya Cave (N55.2994°, E105.4445°) (Fig. 1a) is located on the south-facing shoulder of the Boty river valley, a western tributary of the Lena River, in central Irkutsk Oblast north of Zhigalovo town and ca. 12 km south of Konoshanovo village in southern Siberia, Russia (Fig. 1c). The cave formed under phreatic conditions, in a sub-horizontal 6-to-12 m thick limestone bed of Ordovician age, that is confined below and above by argillaceous sandstones (Filippov, 2000) and is overlain by ca. 20-80 m of sandstone and a thin (10-40 cm) soil. The plateau directly above the cave is relatively flat, with a shallow dry valley that runs southward cutting across the cave (Fig. 1b).

Botovskaya Cave can be entered via three small entrances located at ca. 750 m above sea level on the west-facing slope of a southward-flowing creek that drains towards the Boty River (Fig. 1a). The cave consists of >70 km of horizontal passages (Fig. 1a) created from phreatic corrosion along vertical fissures of bedding planes in a single limestone horizon which is occasionally separated by a sandstone bed into two overlying levels. These passages have a distinctive keyhole shape, suggesting formation through mixing corrosion under phreatic conditions (Filippov, 2000), or possibly by ghost rock formation (Dubois et al., 2014). Most of the cave is filled with unconsolidated sediment which has been excavated in places to reveal a total thickness of 2.8 m (Filippov, 2000). The sediment infill consists of ca. 50 cm of coarse sand, topped by ca. 100 cm of silt-medium sized sand layers, which again are overlain by laminated, but strongly 'brecciated' clay. Close inspection of the sediment profile revealed that the clay was deposited in a low-energy environment, but repeated frost/thaw action linked to the onset and end of glacial periods resulted in fragmentation (brecciation) of the originally laminated clay deposit, which today is characterized by cm-sized, dislocated but internally laminated clasts. While the sand deposits seem to suggest a fluvial flow regime at the end of the phreatic phase in this cave, the clay was likely deposited in near-standing water conditions, possibly at the time when Botovskaya Cave became increasingly disconnected from the groundwater table during the incision of the River Boty. Over the Quaternary, the clay deposit has been brecciated through frost action in this permafrost-affected cave.

Due to its remote location ca. 60 km north of the nearest town (Zhigalovo) the cave remains mostly isolated from human activity besides infrequent research expeditions, which makes Botovskaya Cave well suited for undisturbed environmental monitoring and paleoclimatic studies.

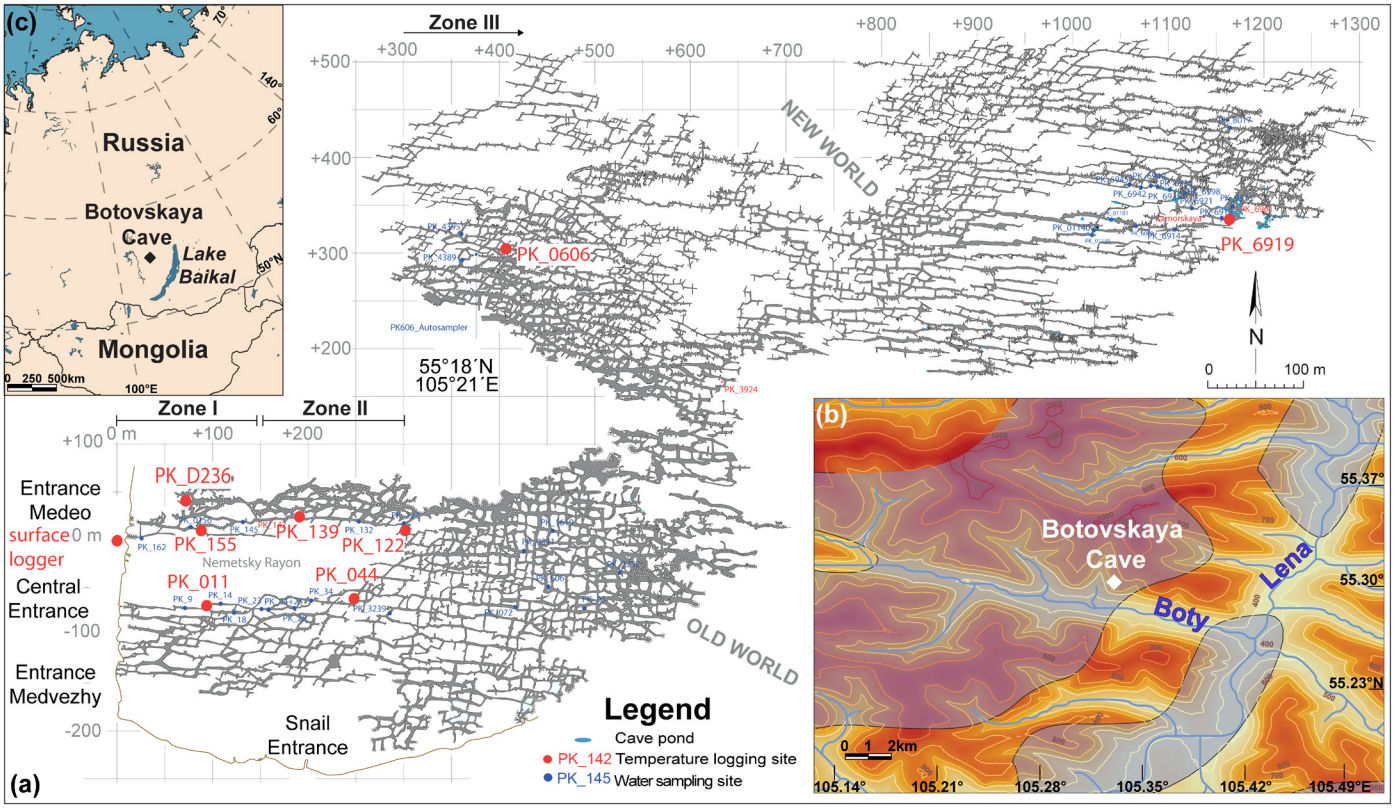

Fig. 1. Botovskaya Cave location and geometry. a) Mapped area of Botovskaya Cave with temperature monitoring sites in red and water isotope sampling sites in blue and (b) region around the cave. Violet shaded areas in (b) highlight sporadic permafrost zones (Obu et al., 2019). c) Botovskaya Cave in continental Eurasia. Base aerial data: © Microsoft.

Southern Siberia is characterized by a continental climate (Dwc climate in the Köppen-Geiger classification; Peel et al., 2007), where summer (JJA) and winter (DJF) mean monthly temperatures are 17°C and -23°C, respectively (averaged from 2010 – 2025), with annual air temperature averaging +1.3 ± 2.4°C. The strong continentality of this region is reflected in the high seasonal temperature contrast. Alongside extreme cold, winters are generally dry and contribute only ca. 10% to the annual precipitation (Fig. 2a). Winter snowfall is limited by the blocking effect of the Siberian High (Cohen et al., 2001; Perşoiu et al., 2019). Summers are significantly wetter, experiencing strong rainstorm events between July and August that contribute ca. 50% of annual precipitation (Fig. 2a). The remaining 40% of precipitation falls across autumn and spring (Fig. 2a). Maximum monthly infiltration (Fig. 2b, c) is observed during late spring, summer, and early autumn (the warm season). Snow covers the cave from early autumn to late spring (Fig. 2a). Snow/winter precipitation will not infiltrate between mid-October to mid-April due to sub-0°C temperatures in the soils (Fig. 2a-c). Part of the accumulated winter precipitation (snowpack height reaches its maximum in February – Fig. 2a) may contribute ca. 13% of annual infiltration between mid-April – May, when surface temperatures rise above 0°C and the ground thaws.

The vegetation occupying the land surface above the cave consists of taiga forests with dark coniferous tree species such as Siberian larch (*Larix sibirica* Ledeb) and Siberian cedar pine (*Pinus sibirica* Ledeb), and some deciduous species such as birch (*Betula* spp. L.), and aspen (*Populus tremula* L.). Undergrowth species include various currant species (i.e., *Ribes rubrum* L. and *Ribes nigrum* L.), as well as lichens and bryophytes (Ponomarev et al., 2016; Margerum et al., 2025). Vegetation around the cave entrances and slopes are less densely scattered, providing only some shading. The cave entrances (Fig. 1a) are exposed to westerly winds associated with the Westerlies year-round.

METHODS & MONITORING PROTOCOL

Microclimatic monitoring operations within and outside Botovskaya Cave have been conducted intermittently from 2003 to 2025, which included both continuous and event-based sampling practices. Grab-sampling, especially of water samples, was confined to field campaigns, conducted either in winter (usually February) or in summer (usually July), only times when the cave location is accessible for expedition. Detailed information about the data loggers used in this study are given in the Supplementary Information Table S1.

Surface and cave air temperature

Surface air temperature was recorded ca. 15 m outside the cave entrance 'Medeo' (Fig. 1; location 'surface logger'), with a Hobosoft UA-001-64 Pendant logger placed ca. 2.5 m above the ground in a shaded section of a tree between 2010-2014 and 2019-2025. Automatic logging of cave air temperature took place at 3-hourly steps over several years at sites (with distance into cave shown in brackets); d236 (83 m), SB_pk0155 (89 m), SB_pk011 (115 m), SB_pk0139 (193 m), SB_pk044 (256 m), SB_pk0122 (302 m), SB_pk606 (507 m), and SB_pk6919 (1212 m) (Fig. 1a) using

Goodsell Systems Ltd Electronic Design solutions and Hobosoft® loggers. The Hobosoft® loggers have a functioning range between -30°C to 50°C with an accuracy and resolution of 0.5°C for temperatures between 0°C and 40°C. All sites are between 0-20 m below bedrock, besides SB_pk606 which is 20 – 40 m and SB_pk6919 which is 60 – 80m. Inside Botovskaya Cave we established a ca. 1200 m long W-E transect of loggers spaced from the entrance to the locations further into the cave (Fig. 1). Note the monitoring sites furthest from the entrance are several hundred meters north and not strictly on a west-east line. This transect helps assessing the characteristics of a temperature gradient and the impact of ventilation on the thermal regime of the cave.

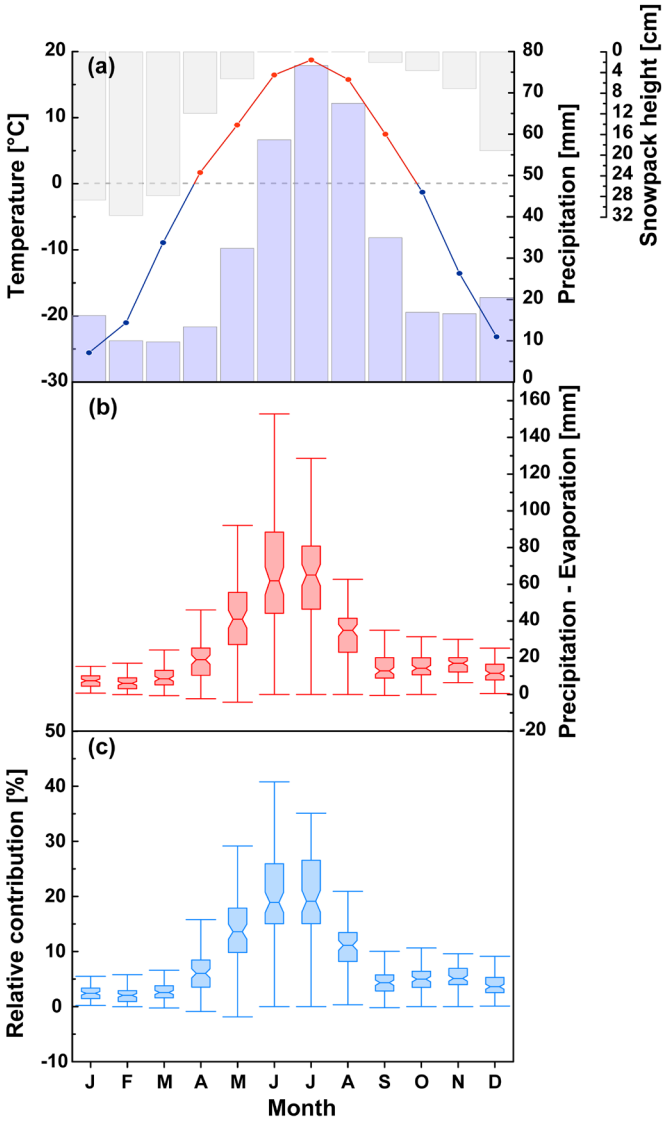

Fig. 2. Climatic conditions at Botovskaya Cave. a) Average monthly surface temperature and precipitation, measured 2 m above ground 2010 – 2025 at Zhigalovo Meteorological station (no. 30521), source: https://rp5.ru/Архив_погоды_в_Жигалово. Temperature below 0°C is blue and above 0°C in red. Grey-shaded bars indicate mean monthly snowpack height. b) Mean monthly infiltration (precipitation – evaporation) averaged from 1937 – 2025 (box-whisker plots with median, interquartile range, maximum and minimum). c) Mean monthly contribution to annual infiltration from 1939 – 2025 (box-whisker plots with median, interquartile range, maximum and minimum). Data for (b) and (c) are sourced from Muñoz Sabater (2019): ERA5-Land hourly data from 1950 to present. Copernicus Climate Change Service (C3S) Climate Data Store (CDS). https://doi.org/10.24381/cds.e2161bac (accessed on October 15, 2025).

Cave air CO_2 concentration, relative humidity, and temperature

Cave air CO_2 concentrations (ppm), atmospheric pressure, relative humidity, and temperature, were measured between mid-February to mid-August 2022 at site SB_pk606, ca. 507 m inside the cave (Fig. 1) using a Goodsell (www.goodsellsystems.co.uk) CO_2 data logger at 3 hourly intervals. The CO_2 concentration was measured via a SCD30 sensor module with an accuracy of ±30 ppm and temperature stability of ±2.5 ppm/°C. The combination of these parameters within the deep and hydrologically active area of the cave helps the understanding of cave ventilation dynamics due to the intrinsic relationship of these parameters to cave air mass movement. Relative humidity was also recorded at site d236 with a Hobosoft® Pro RH/temp logger (with identical specifications to the Hobo Pro Temp loggers used at the sites mentioned in subsection 'surface and cave air temperature').

Dripwater collection

To collect dripwater samples for subsequent stable isotope ($\delta^{18}O$ and $\delta^{2}H$, d-excess) analysis we deployed a custom-built automatic dripwater sampler at site SB_pk606. This device was developed at ETH Zurich and then re-designed at Northumbria University and consists of a rotating carousel system that holds 54 vials, which allowed us to collect weekly dripwater samples. After collection of water over a week, each sampling vial is closed automatically to avoid evaporation and/or mixing of waters of individual samples. A funnel and HDPE tubing guide dripwater from an active drip site into a vial. The carousel rotates at the end of a given sampling week. Additionally, dripwater and cave pond water samples were collected manually in different locations in the cave during expeditions.

Water samples from local and regional precipitation, rivers Boty and Lena were collected manually during multiple expeditions between 2003 to 2022 (see Fig. 1a for sampling locations, and Supplementary Table S2 and S3 for water isotope data acquired). These samples were usually taken during winter expeditions, but several samples were collected in summer. Water isotopes were analyzed using both, isotope ratio mass spectrometry (IRMS) and a Cavity-Ring-Down-Spectroscopy (CRDS) employed at the Alfred Wegener Institute for Polar and Marine Research in Potsdam. A Finnigan MAT Delta-S IRMS with two equilibration units was used for the online determination of hydrogen and oxygen isotopic composition. For CRDS analyses an aliquot of about 2 µl of water is injected into a Picarro L2130i Isotopic Water Liquid Analyzer and analyzed following the procedure of (Juhls et al., 2020). This process is repeated 6 times resulting in final sample $\delta^{2}H$ and $\delta^{18}O$ values (referring to the permil difference related to V-SMOW). These values are corrected for drift and memory effects. Results ($\delta^{2}H$ and $\delta^{18}O$) are reported in permil (‰) relative to the Vienna Standard Mean Ocean Water (VSMOW) standard (Meyer et al., 2000; Juhls et al., 2020). The external errors for standard measurements of $\delta^{2}H$ and $\delta^{18}O$ are better than ± 0.8 ‰ and ± 0.1 ‰,

respectively. Dripwaters from the autosampler (site SB_pk606) were measured using a WS-CRDS Picarro L2140i analyzer at the Institute of the Earth's Crust in Irkutsk, employing methods from Ekaykin (2016). Results are given in the Supplementary Information Table S3.

Meteorological data

Meteorological data, collected between 2010 – 2025 at 3-hourly resolution, is available from Zhigalovo meteorological station (station ID: 30521), including temperature at 2 m above ground level, minimum and maximum air temperature, precipitation amount, minimum soil surface temperature overnight, and snowpack height (source: http://rp5.ru, accessed August 31, 2025). These instrumental records provide a robust basis to characterize the microclimate and hydrological dynamics near Botovskaya Cave at diurnal to decadal timescales.

To calculate maximum monthly infiltration of precipitation and the monthly contribution to annual infiltration (as seen in Fig. 2b, c), we use potential evaporation, evaporation, dew point, and surface temperature data (1939-2025) from Muñoz Sabater (2019) and monthly average surface temperature, precipitation, and max precipitation (mm) from 1937 to 2025 from the Daily Global Historical Climatology Network (Menne et al., 2012; version 3.32 accessed: August 31, 2025). We used the Haude formula and a monthly empirical factor for spruce forest to derive average monthly potential evapotranspiration (Haude 1955). The vapor pressure deficit was taken from the difference between saturation vapor pressure and actual vapor pressure, following the FAO Penman-Monteith formula (Allen et al., 1998).

RESULTS

Surface air temperature

Surface air temperature data recorded immediately outside the cave system (at the surface logger site; Fig. 1a) between 2011-2014 and 2019-2025 shows characteristic annual and seasonal trends of warm summers and very cold winters (Fig. 3a). The coldest temperatures were recorded in December 2010 of -40°C, and warmest in June 2022 of 37°C. The highest diurnal temperature variations of up to 10°C are observed in March. In spring, the 0°C threshold is usually crossed in early to mid-March, although nighttime temperatures can still reach below 0°C well into late May. Temperatures below 0°C are usually not seen again until mid-late September, and temperatures remain negative from early November onwards.

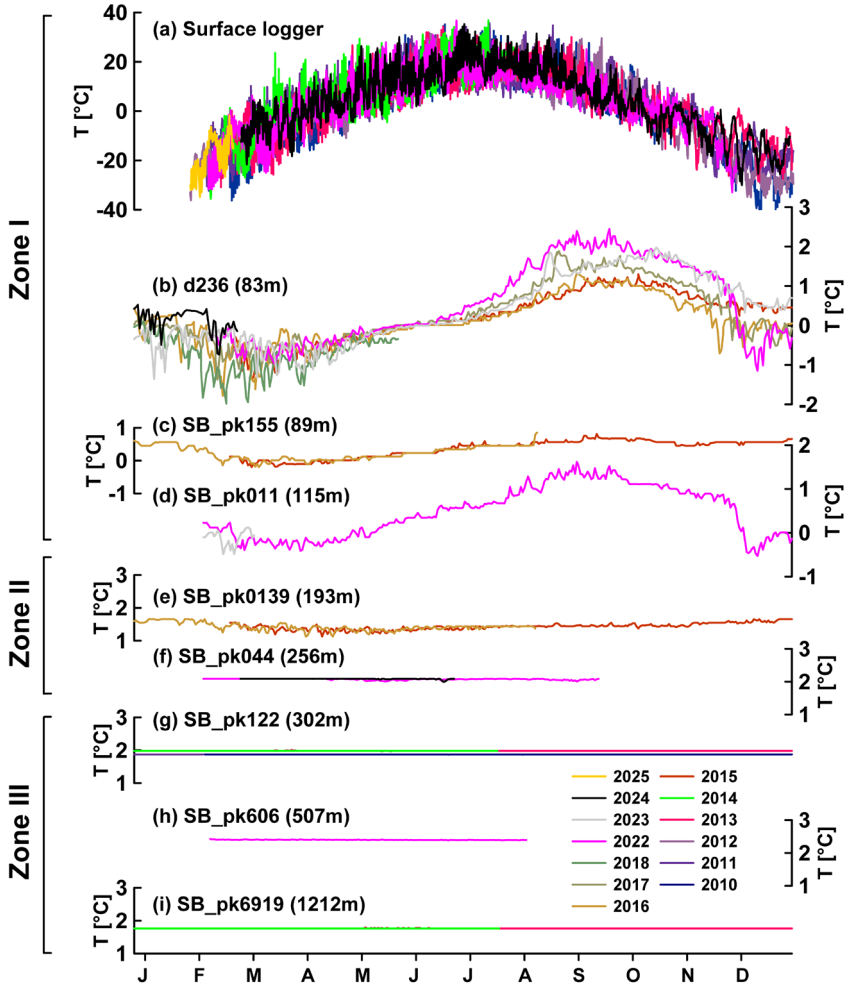

Fig. 3. Monthly temperature variations recorded above and in Botovskaya Cave. 3- to 6-hourly temperature records from (a) the surface, (b-d) sites d236 and SB_pk155 near the entrance, and SB_pk011 in zone I (within 150 m of the entrance), (e-f) central sites SB_pk0139 and SB_pk044 in zone II (150-300 m from entrance), and (g-i) sites deep in the cave: SB_pk122, SB_pk606, and SB_pk6919 in zone III (>300 m of entrance). Because multiple years are recorded (see legend), all records were projected onto a single year. Multi-annual datasets from individual sites generally replicate well. Temperature variance declines with distance from the cave entrance (from sites b to i).

Cave air temperature

Cave air temperatures are much less variable compared to surface air temperature and show low variance throughout the year (Fig. 3b-i and Supplementary Fig. S1). Sites near the entrance (Fig. 3b-e) show a seasonal range between -2°C and +2.5°C, in contrast to the deeper zones of the cave (>300 m from the entrance) where air temperatures are slightly higher and range from +1.7°C to +2.4°C (Fig. 3f-i). The most stable temperature is found in the cave sections furthest from the entrances (Fig. 3f-i). Site d236 (83 m from entrance) shows the lowest in-cave air temperature of -1.9°C in February and March, but also the highest cave air temperature reaching +2.4°C in late September (Fig. 3c). Site SB_pk606 (507 m from the entrance; Fig. 3h) is the warmest site with temperatures remaining at 2.4 ± 0.01°C. There is a lagged cave air temperature response to surface temperature changes with increasing distance from the cave entrance. Near entrance sites show an ca. 1-month delay from maximum seasonal surface temperatures. With increasing distance into the cave (to SB_pk0139), this lag extends to a ca. 6 months, with highest in-cave temperatures reached at site SB_pk0139 only in early December. Temperature changes are negligible past a distance of 300 m from the entrance.

This temperature-distance relationship can be used to divide the cave into three zones I, II, and III, along a West-East transect with increasing distance from the main entrance (Medeo) (Fig. 1). Zone I includes the cave section between 0 and 150 m from the entrance, with a temperature variation of >1°C, zone II is 150 to 300 m from the entrance with temperature variation of 0.1-1°C, and zone III is >300 m from the entrance with temperature variation of <0.1°C (Fig. 3).

Cave air CO_2 changes

Cave air CO_2 concentration was measured at site SB_pk606 (Fig. 1) from February to August 2022 and varies around a mean of 852 ± 130 ppm (Fig. 4). Between February and early May, average 12 hourly CO_2 changes were notably greater (106 ppm) than mid-May to late August (28 ppm) (Supplementary Table S4). In addition, CO_2 concentration in the cave air gradually declined until the first week of May, after which an increasing trend set in (Fig. 4a, b). In February, CO_2 values are higher (965 ± 111 ppm) than in both spring (March-May, 824 ± 139 ppm) and summer (June-August, 905 ± 70 ppm).

The average CO_2 value for each 3-hour interval for each of the recorded months (Fig. 4c) reveals more pronounced winter – spring CO_2 variability compared to relatively stable summer CO_2 levels. February and April present similar dynamics, where peak CO_2 values are observed at night (00:00) and begin to decline around 03:00 – 06:00, then rising again around 12:00-15:00. These trends are more significant in April which presents a CO_2 decline of 100 ppm (from 875 to 775) from 00:00 to 12:00. In March, almost opposite CO_2 trends are found, with peak CO_2 levels reached at 15:00 which then decline until a minimum is reached at 06:00. During spring and summer (May – August) CO_2 values generally increase but show little diurnal variation (CO_2 = 811 ± 28 ppm).

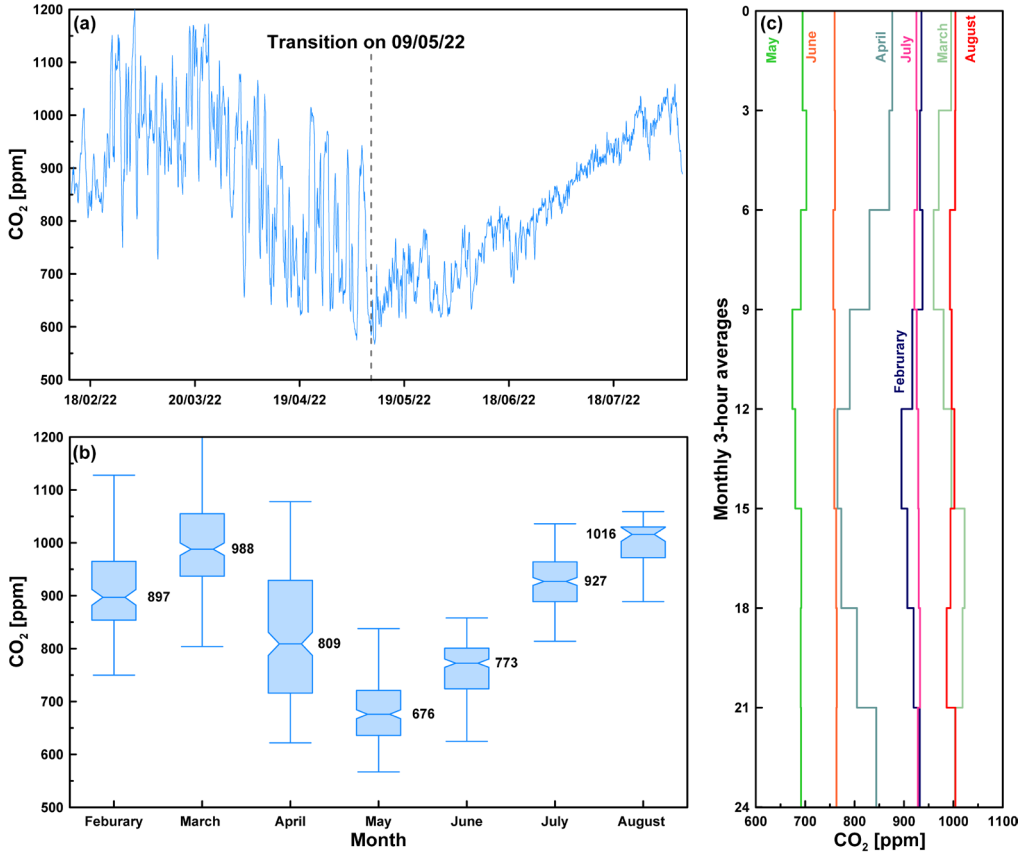

Fig. 4. CO_2 results at site SB_pk606 from February – August 2022. a) Three-hour CO_2 measurements show that concentrations decline during the winter and spring months, followed by a notable transition beginning on 09/05/22, when daily variability decreases and CO_2 levels begin to increase. b) Box-whisker plots of the same data, with mean monthly variation and interquartile ranges of CO_2. c) Average 3-hourly change of CO_2 per month shown with winter (blue), spring (greens), and summer (reds). Winter and spring diurnal variation are greater than summer.

Water isotopes

A total of 75 precipitation, dripwater, and pond water samples have been collected for stable isotope analysis in and above Botovskaya Cave. Twenty-four precipitation samples, collected near the cave, define a Local Meteorological Water Line (LMWL) for our site (Fig. 5a). The average $\delta^{18}O$ of dripwater (-17.8 ± 0.09‰) and weighted average $\delta^{18}O$ of precipitation (-17.8 ± 0.05‰) fall within error on the LMWL. The weighted average of $\delta^{18}O$ precipitation was calculated by identifying the relative contribution of precipitation in summer (50%) to all other seasons (50%) (shown in Fig. 2c) across multiple years and thus applying seasonal 'weight' to the average $\delta^{18}O$ of precipitation. Winter precipitation is characterized by very low $\delta^{18}O$ values between -35 and -21‰ and $\delta^{2}H$ values that range from –273 to -162‰, while summer rainfall $\delta^{18}O$ values range from -15 to -5‰ and $\delta^{2}H$ range from -116 to -54‰.

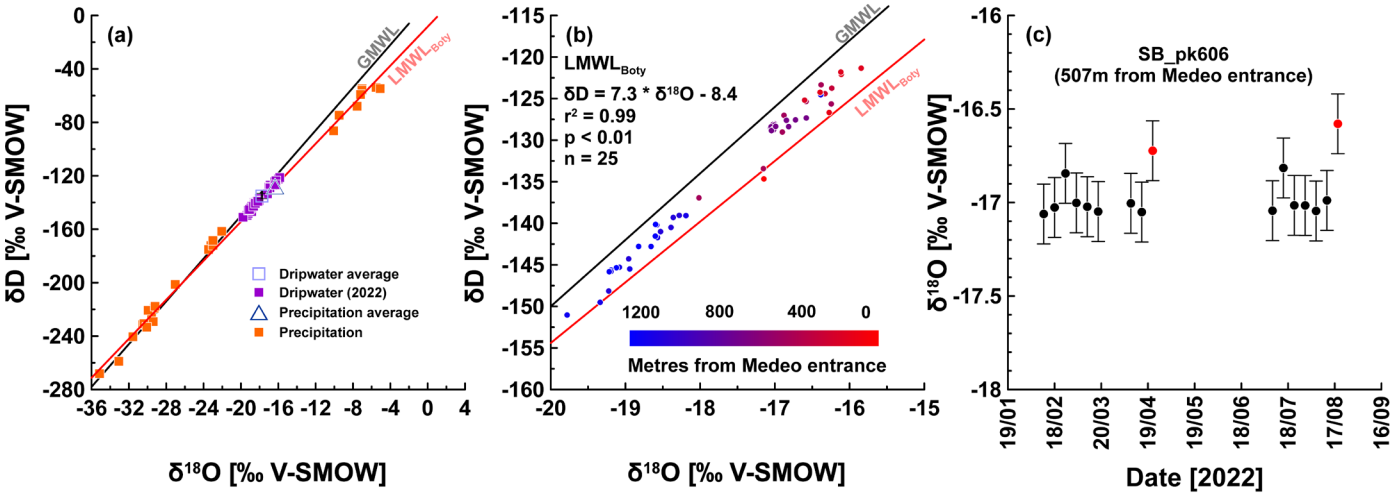

Fig. 5. Summary of $\delta^{18}O$ and $\delta^{2}H$ in precipitation and in cave waters, and link to distance from cave entrance. a) Precipitation (orange), and dripwater (purple), with average values for precipitation and dripwater are shown with 2σ errors. The LMWL ($\delta^{2}H = 7.3 \times \delta^{18}O - 8.4$) (red line) is based on precipitation samples from around Botovskaya Cave and the GMWL ($\delta^{2}H = 8 \times \delta^{18}O + 10$) (black) is from Craig (1961). b) Drip and pondwater $\delta^{18}O$ become significantly more negative with increasing distance from the entrance (distance is measured as the crow flies, not along passages). c) Dripwater isotopic composition at site SB_pk606 (507 m in the cave), collected with the autosampler, remains near-constant, with only few samples showing less negative values. Data are shown with 2σ errors. Red symbols denote samples with little water and spurious results.

Drip-and Pond water $\delta^{18}O$ from across Botovskaya Cave (Fig. 5b) vary ca. 4 ‰ between -15.8 to -19.8 ‰, and $\delta^{2}H$ ranges from -118.8 to -151‰, with mean $\delta^{18}O$ and $\delta^{2}H$ values of -17.6 ± 1.1‰ and -133.7 ± 8.9‰ (2σ), respectively. The annual average $\delta^{18}O$ value in dripwater is -17.8 ± 0.09‰ (2σ), which is within uncertainties indistinguishable from the weighted average value observed in precipitation of -17.8 ± 0.05‰ (Fig. 5a). Dripwater and pond water isotope ratios change significantly ($r^2 = 0.74$, $p < 0.0001$) with distance to the western limit of the cave (measured relative to the main cave entrance Medeo, Fig. 5b), with $\delta^{18}O$ decreasing ca. 1‰ every 500 m eastward. This relationship explains the large total range of ca. 4‰ in dripwater and pond water $\delta^{18}O$ from different sites in Botovskaya Cave (Fig. 5b).

At site SB_pk606 we find constant (within analytical uncertainties) $\delta^{18}O$ values in dripwater collected at roughly weekly intervals over ca. 6 months using the automatic sampler (average = -17.01 ± 0.06‰, N = 13) (Fig. 5c). Three samples were identified as outliers (with values -16.72 ± 0.08‰; -16.82 ± 0.08‰ and -16.58 ± 0.08‰) (red samples: Fig. 5c). A sampling gap occurred between April – July due to a malfunction of the autosampler (i.e., jammed carousel). Dripwater and pondwater samples provide statistically indistinguishable results, indicating absence of secondary evaporation in the cave.

Precipitation and infiltration

Calculated infiltration into Botovskaya Cave is highest in summer, with a mean of 62 and 65 mm of infiltration in June and July, respectively (Fig. 2b). The lowest potential infiltration is calculated for February (6 mm, of which none would infiltrate given the frozen ground, nor in other winter months were temperatures below 0°C).

The relative mean monthly contribution to annual infiltration (Fig. 2c) showed similar results, where 38% of infiltration is likely to occur in both June and July. Collectively, 63% of infiltration occurs between May – September, and the remaining 37% occurs between October – April. Sub-zero temperatures between October – March (Fig. 2a) are not considered in the calculations for infiltration and that the window of effective infiltration is only open between April and September. This suggests that 63% of the total annual infiltration is supplied during the warm season (May-September).

DISCUSSION

Surface and cave temperature regimes

Due to the high continentality, surface temperatures vary from very cold (on average -22°C) in December – February, to warm (on average 16°C) temperatures in June – August. While no frost is documented during the warm season (mid-May to mid-September), in autumn, soils above the cave are repeatedly frozen and thawed, as daytime and nighttime temperatures fluctuate around 0°C between mid-September until late October. When both daytime and nighttime temperatures drop below 0°C in early November, the ground remains permanently frozen until late April

– early May. A similar dynamic pattern occurs in spring, when daytime temperatures climb above 0°C in early March, but freezing still occurs at night. This temperature regime governs the infiltration potential which is limited to the window of unfrozen soil and higher warm season precipitation (mid-May to mid-September). However, infiltration might be possible over the daytime from as early as March and as late as November if precipitation falls as rain rather than snow.

The small dimensions of the cave entrances and passages and the inertia of the bedrock both limit sub-surface temperature variation in the cave. The decreasing impact of seasonal variations in surface temperature on cave air temperature is well reflected in the temperature variations observed in the three zones delineated along the monitoring transect (Figs 1a and 3). With increasing distance from the western edge of the cave (from zone I – III), in-cave temperatures increase and become increasingly stable.

Narrow cave passages encourage air to reach the temperature of the surrounding rock, which limits both convective heat transfer (Gabrovšek, 2023) and air exchange with the surface, minimizing temperature swings in zones II and III, which are instead predominantly affected by the conductive heat transfer of mean annual air temperatures (MAAT) through soil and rock (Smerdon et al., 2003, 2004; Rau et al., 2015). Located furthest from the entrances, zone III is the warmest zone of the cave and maintains temperatures between 1.8 ± 0.01°C and 2.5 ± 0.01°C (1 standard deviation over the recorded period), with no seasonal variation (Fig. 3). Since the loggers used are only accurate to ± 0.5°C the results indicate thermal stability at the level of instrumental accuracy and resolution. The temperature in this zone agrees with the MAAT recorded by the surface logger (Fig. 1, +1.3 ± 2.4°C). Seasonal temperature variations are absent in zone III (at least within the accuracy of the loggers used), and we posit that zone III responds only to multi-decadal – centennial-scale surface temperature changes.

Precipitation and its isotopic composition

The precipitation regime above Botovskaya Cave is governed by late spring to autumn rainfall which delivers ca. 75% of the annual precipitation, and a relatively small contribution of winter snowfall to the annual total (Fig. 2a). With ongoing global warming, the infiltration window (currently mid-May to mid-September) is likely to widen together with the increasing length of the warm season (Wang et al., 2021). Effective infiltration (i.e., precipitation minus evapotranspiration and surface runoff) (Fig. 2b) that feeds the dripwater is governed by environmental conditions such as surface and ground temperatures, vegetation density/type, soil type/porosity, and elevation (Haude 1955; Cui et al., 2019). At Botovskaya Cave, effective infiltration occurs predominantly in the warm season, although somewhat limited by evapotranspiration, while sub-zero temperatures in the cold season prevent infiltration.

The low input to average annual precipitation of winter, autumn, and spring (50%) relative to summer precipitation (50%) reflects the influence of the winterly Siberian High, an anticyclonic high-pressure cell that is intensified during winter (Cohen et al., 2001; Perşoiu et al., 2019; Kostrova et al., 2020). The Siberian High restricts and deflects moisture transport into southern Siberia, resulting in very dry winters relative to the summer period. When the Siberian High weakens with increasing temperatures, and its blocking effect for moisture transport into the region is reduced, the prevailing Westerlies can supply more moisture to the study region. Summer rainfall is fed further by significant recycling of regionally evaporated moisture, and the summer heat in this highly continental region results in strong convective thunderstorms (Kostrova et al., 2020). However, to provide a better understanding of seasonal infiltration, not only dripwater composition but also regular drip rate monitoring is required.

The $\delta^{18}O$ and $\delta^{2}H$ values of precipitation at Botovskaya Cave differ significantly between very negative winter (snow) and less negative summer (rain) (Table 1) and closely match the seasonal values from Irkutsk reported by Kostrova et al. (2020). The d-excess values are higher in winter and lower in spring and summer (Table 1), mirroring enhanced secondary evaporation during moisture recycling in summer (Kostrova et al. 2020). Given these similarities we argue that Irkutsk and Botovskaya Cave experience essentially the same temperature and precipitation regime and continentality.

Table 1. Averages of seasonal amount-weighted mean $\delta^{18}O$, $\delta^{2}H$, and d-excess in precipitation observed at Botovskaya Cave between June 2009 – February 2022. Precipitation isotope results from Kostrova et al (2020) originating from Irkutsk are also shown in italics.

	$\delta^{18}O$ weighted mean [‰ VSMOW]	**$\delta^{2}H$ weighted mean [‰ VSMOW]**	**d-excess [‰]**	**Average precipitation [mm] (as annual %)**	**Average dripwater $\delta^{18}O$ [‰]**
Winter (DJF)	-28.5 ± 0.04 *-28.6 ± 2.1*	-218.8 ± 1.6 *-222.1 ± 2.1*	9.43 *6.5*	37.2 (11)	-17.6 ± 1.1
Spring (MAM)	-16.8 ± 0.04 *-16.8 ± 3.4*	-135.7 ± 1.1 *-128.6 ± 26.4*	-1.05 *5.9*	39.6 (12)	
Summer (JJA)	-11.2 ± 0.04 *-11.9 ± 1.4*	-86.6 ± 1.4 *-92.4 ± 10.6*	3.16 *5.3*	199.6 (57)	
Autumn (SON)	-18 ± 0.04 *-20.6 ± 3.8*	-135.1 ± 1.7 *-157.8 ± 27.9*	9.13 *5.5*	68.4 (20)	

Using backward trajectory modelling, Kostrova et al. (2020) showed that the origin of moisture varies seasonally. During autumn and winter, more negative $\delta^{18}O$ and high d-excess values in precipitation are linked to moisture transport from high latitudes and the Arctic, while in summer moisture with less negative $\delta^{18}O$ and lower d-excess values is delivered via the Westerlies from the Atlantic Ocean and

western Siberia, or from regionally recycled moisture. While today the Westerlies and regional recycling contribute most to the precipitation above Botovskaya Cave, a warmer Arctic coast with extended sea ice free summers might, in the near future, increase the contribution of moisture from the Arctic, especially in autumn. Higher contribution of Arctic moisture would lead to lower $\delta^{18}O$ and $\delta^{2}H$ in precipitation, and ultimately in the dripwater.

Cave ventilation dynamics

Cave ventilation is an important factor for the precipitation of speleothems and the sensitivity of environmental proxies in them. Increasing airflow intensifies cave air exchange and removal of carbon dioxide brought into the cave with the dripwater. Stronger ventilation thus lowers cave air CO_2 and increases CO_2 outgassing rates from incoming waters, thereby encouraging precipitation of carbonates (Kukuljan et al., 2021). The ventilation dynamics of a given cave depend strongly on the geometry of the cave and the number, size, and orientation of the entrance(s) (e.g., Baldini et al., 2006.; Breitenbach et al., 2015; Ridley et al., 2015; Riechelmann et al., 2019). Multiple physical processes, such as external wind-induced airflow, chimney circulation, convection, and water-induced flow, can aid air circulation (Fairchild and Baker, 2012; Riechelmann et al., 2019; Kukuljan et al., 2021; Gabrovšek, 2023), and seasonal changes of surface air temperatures, where the density gradient between surface and cave air can enhance airflow (James et al., 2015; Box et al., 2025). Many of these examples are not feasible in Botovskaya Cave due to its horizontal geometry, narrow passages, length, and interconnectivity of passages, which conspire to restrict and weaken air movement. Wind is restricted to the entrance areas and can only be regarded a secondary ventilation factor, and chimney circulation (where the density difference of subsurface vs. surface air drives airflow) is restricted by the narrow (on average 1 m wide) and low (often 1.5 m high, with a maximum of ca. 3 m) horizontal passages. Water entrainment, which requires significant water flow into the cave, is also not possible at the position of Botovskaya Cave on the hillslope of the Boty River. Slow density-driven air movement in these narrow passages is the main process for cave ventilation.

Cave CO_2 is sourced from the burozem-like soils above Botovskaya Cave (Golubtsov et al., 2023), which are supplied by litter/organic carbon from mixed coniferous-deciduous taiga forest known for their high carbon production and sequestration capacity (Dsouza et al., 2025). Soil organic carbon (SOC) concentration is governed by permafrost occurrence, soil moisture (Schiedung et al., 2022), and temperature (Sawamoto et al., 2000), with the SOC budget depending on the season and freeze-thaw dynamics (Gao et al., 2022). The SOC concentrations in semi-decomposed burozem soils are estimated to range between 50 and 75 g/kg during the warm season, and 35 to 50 g/kg in the winter season, with SOC increases aligning with the number of frost-thaw cycles, and organic carbon is released into the soil during spring thaw (Sawamoto et al., 2020; Gao et al., 2022). We can infer from the summer maximum of effective infiltration that water is actively entering the soil, sub-soil and epikarst during the summer and autumn and thus brings DIC into the cave.

Despite stable thermal conditions in zone III (Fig. 3), the observed high winter CO_2 variation and spring decline in CO_2 seem to indicate some kind of ventilation, while the rising CO_2 level in summer suggests active CO_2 recharge (Fig. 4a). We propose that the summer CO_2 recharge may originate from higher vegetation and microbial activity in the soil, which is transported into the cave by higher infiltration (Pla et al., 2016). We suspect that cave ventilation, prompted by air density, snowpack height and temperature contrasts between surface and cave, drives the observed CO_2 changes in zone III. Using monitoring data from the 2022 fieldwork, below we evaluate the role that seasonal ventilation dynamics play on changes in cave air CO_2.

Winter ventilation

In winter and until early spring, cave CO_2 is high and variable, revealing that deep cave (zone III) air is poorly ventilated but not stagnant and maintains some connection to the dynamics on the surface. From mid-autumn (late September) until spring (April), when surface temperature is below 0°C, snow blankets Botovskaya Cave (Fig. 2a) and covers the cave entrances. This snow cover insulates the ground and the cave against temperature changes, but not entirely against CO_2 flux through the entrances and vertical joints and fissures along which gas flow is possible. The rising cave air CO_2 likely results from CO_2 degassing from dripwater. In Botovskaya Cave, drips remain active during winter as the lower epikarst remains unfrozen. The high (although variable, with daily – weekly changes of ca. 100 ppm, Fig. 4a) winter cave air CO_2 level may result from freezing of water in the shallow soils and near-surface epikarst (Fang et al., 2024) which contains CO_2-rich waters from the warm season. The infiltrating water freezes downward with continued frost which would push the dissolved CO_2 downward into the unfrozen water, which continues its journey into the cave where it outgasses CO_2. The high variability of CO_2 concentration in the cave air might reflect the impact of severe freezing periods (Fig. 6) that push the freezing front deeper into the epikarst (which in turn could increase the CO_2 concentration in the remaining fluid phase). Falling CO_2 levels in winter likely result from transport of (relatively warm) cave air through the vertical joints that connect to the surface; this notion is supported by mounds of hoar frost crystals that have been observed above the snowpack which form from the exhalation of moist (and warm relative to surface air) cave air during winter (Supplementary Fig. S2). These mounds are up to 1 m tall and 20-30 cm wide. However, the snow covering the entrances and frozen water in the overlying soil and epikarst leave only the largest joints near the western cave sections as pathways for moist, CO_2 enriched cave air to exit the cave (Fig. 7a).

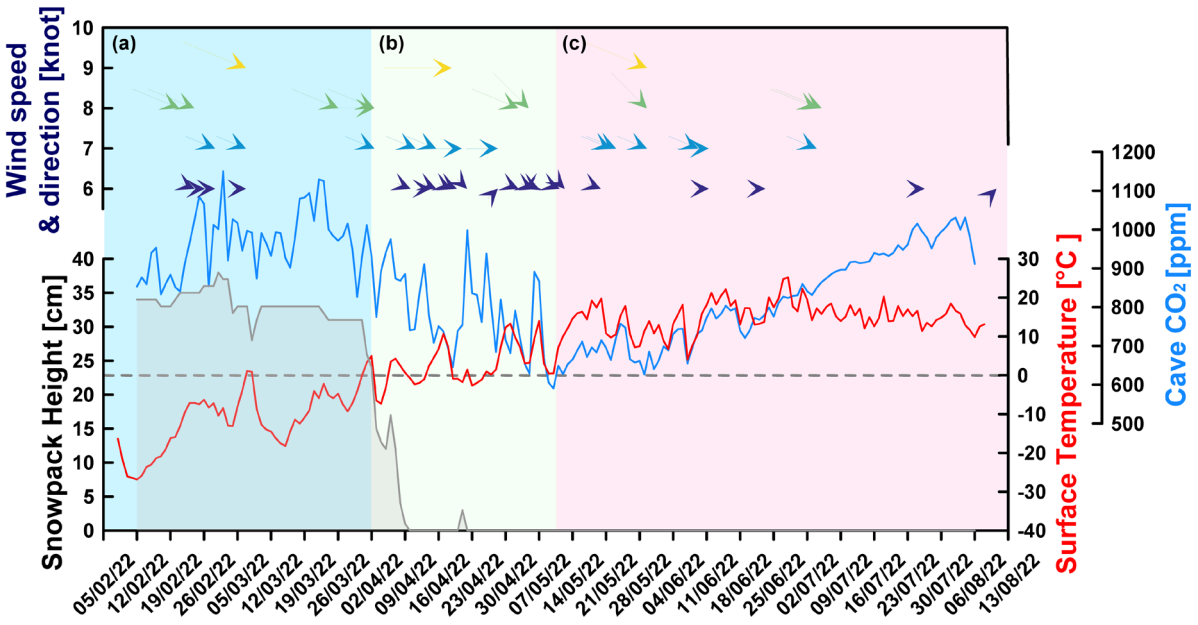

Fig. 6. Links between cave CO_2 dynamics, surface temperature, wind speed and direction, and snow cover. a) Winter (shaded blue); high CO_2 levels are maintained due to continued influx of CO_2 with dripwater, but restricted air flow from the cave via joints and entrances. b) Spring (green shade); more frequent and stronger winds, rising surface temperature and melting snow help ventilation and CO_2 removal from the cave. c) Summer (pink); restricted ventilation results in rising CO_2 concentration in the cave.

The lack of thermal response in zone III may be due to very slow conduction through bedrock and limited convection of air given the small elevation differences in the cave. It is more likely that cave air moves along vertical fissures in the cave ceiling that facilitate warm air rising out of the cave during winter.

Spring ventilation

In spring (March – April), surface temperature rises, and significant diurnal temperature changes are frequent (10°C within 24 hours) (Fig. 6b). Daytime temperatures stabilize above 0°C only in early May. Cave air CO_2 gradually falls from the winter maximum of ca. 1000 ppm to a minimum of ca. 600-650 ppm by early May. This might reflect an increased ventilation regime during springtime, invigorated by the dynamic diurnal temperature regime, when daytime surface air is already positive and much warmer than cave air, while nighttime temperatures are often well below zero and lower than cave air temperature (Fig. 7b, c). The resulting air density gradients between cave and surface vary considerably and allow air transport out of the cave at night (when warmer cave air exits the cave upwards) (Fig. 7c).

Ventilation is further facilitated by the establishment of positive daytime temperatures and melting of the accumulated snow which facilitates better air exchange via the re-opened cave entrances. In March when snow still covers much of the cave, cave air CO_2 sinks in the night/early morning hours when outside temperatures are much cooler than in-cave temperature. In April, this dynamic shifts to midday CO_2 minima and nighttime maxima, which may relate to the weaker gradient between surface and cave in the afternoon compared to a stronger gradient at night. While the midday low CO_2 levels in Botovskaya Cave can be explained by the same mechanism of warmer cave air relative to surface air, the nighttime maxima require explanation. We suggest that this behavior might result from enhanced transport of soil CO_2 into the cave after the soil and top of the epikarst thaw. Soil-derived CO_2 from the previous warm season, stuck in the frozen ground would now be released and transported with meltwater into the cave, likely with a lagged response to daytime warming that results in an afternoon – evening CO_2 maximum.

With snow-free cave entrances, the cave is also more exposed to windier spring weather (relative to winter) which may assist cave ventilation. Both April and May are characterized by frequent westerly winds with higher average wind speeds, relative to other months (Fig. 6). Wind-induced ventilation has been reported from other caves (e.g., Riechelmann et al. 2019) and with stronger westerly winds directly facing cave entrances, ventilation could displace internal entrance air (reflected in the more variable temperatures at site d236), and faster replacement of cave air by surface air, ultimately resulting in a decline in cave air CO_2. This mechanism is only relevant for zone I, because the cave geometry suppresses air flow drastically with distance from the entrance.

Furthermore, the presence and absence of snow likely also play a role in the apparent CO_2 changes, especially during the transition period (May 9th) when cave air CO_2 levels stop declining and shortly afterwards begin to rise. We find a good correlation (r^2 = 0.5) between the snowpack height and cave CO_2 suggesting that the abundance of snow limits ventilation and supports the winterly rise in cave air CO_2 (which is continuously supplied via active drips). A thicker snowpack helps to seal the entrances and joints to the surface. However, because snow is a porous barrier and its effectiveness strongly depends on thickness and compactness, where slight changes to this snow layer could result in high variability in gas exchange with the surface, and thus cave CO_2. Snowpack height data suggests most snow is cleared by early April when surface temperature begins to rise above 0°C (Fig. 6). It is

likely that the snowpack around the cave entrances is maintained for a longer period and might only melt in early May. This is due to the rough terrain at the entrances where the limestone layer strikes out, and frequent reversal to sub-zero surface temperatures (especially at night) in springtime.

The lowest cave air CO_2 concentration is observed in early May (Fig. 3b, c, Fig. 6). This time marks the transition from high to low (diurnal to monthly scale) CO_2 variability in the cave. In early spring, the cave air is warmer than surface air (at least during the night and mornings) and with the snow cover now removed, air can more freely exit the cave. This thermally driven ventilation is further enhanced by the thawing of any ice in the crevasses and joints through which additional airflow is now possible (Fig. 7b). Since production of CO_2 in the soil is still very limited at that time of year, effectively more CO_2 is removed from the cave and the CO_2 level declines. The low CO_2 levels between May and June may further reflect reduced dripwater and CO_2 flux into the cave during these months. An 11-week gap in the autosampler dripwater dataset (Fig. 5c) would support this notion, as these vials remained empty and the sample vials bordering the missing May – June sampling dates did not completely fill. Drip rates may be reduced in response to lower infiltration right after draining of the freshly thawed ground (which trapped water from the previous warm season) (Fang et al., 2024) and prior to the onset of summer season rainfall. Elucidating this tentative link between dripwater and CO_2 dynamics requires currently unavailable drip rate information.

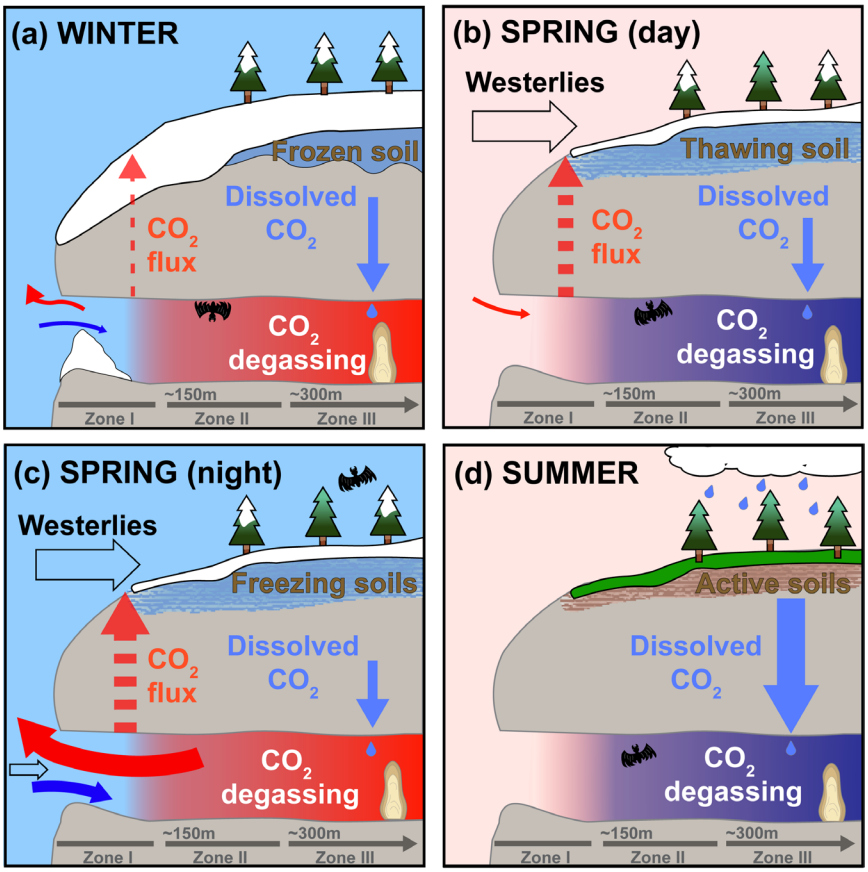

Fig. 7. Schematic detailing inferred seasonal ventilation conditions in Botovskaya Cave. a) Presents low level winter ventilation due to stagnation of cave air in response to closed cave entrances. b) Spring daytime ventilation declines with warmer surface temperatures, then (c) increases due to cold air movement helped by westerly winds. d) Weakened summer ventilation due to establishment of near-stagnant cold cave air, and CO_2 recharge from increased soil activity and dripwater influx.

Summer ventilation

At the onset of summer (mid-May to June), cave air CO_2 is lowest (650-700 ppm), and surface air temperatures regularly exceed 20°C. In later spring/early summer (in our record between mid-May and early June, Fig. 3) average daily surface air temperature is close to the average cave air temperature, resulting in a minimal thermal gradient between cave air and surface air temperatures, and consequently reduced cave ventilation that limits diurnal cave air temperature changes and prevents in cave CO_2 concentration to reach surface air level. The timing and length of this period depends on surface dynamics and varies on interannual scale. Two main mechanisms converge to gradually increase cave air CO_2 as observed from June to late August (Fig. 6). First, high and frequent rainfall, which may initially force some pockets of soil CO_2 into the atmosphere, increases drip rates and saturates the soil and epikarst once more, providing more opportunity for CO_2 uptake in the soil and subsequent degassing from dripwater in the cave. The increasing biological activity and high rainfall over summer intensify plant and microbial respiration in soil and raise CO_2 levels in the soil. High effective infiltration during these months (Fig. 2) helps transfer that CO_2 into the cave system while, concurrently, cave air CO_2 increases due to significantly suppressed ventilation. The cave is increasingly colder relative to the surface (Fig. 6) and given its horizontal layout with few and small

entrances, acts like a cold trap where the cold, dense cave air remains stagnant in the passages. The cold cave air is unable to rise through the joints in the epikarst and ventilation is minimized (Fig. 7d). Finally, the prevailing westerly winds weaken during summer and thereby minimize the displacement of cave air in zone I. This process facilitates more stable temperatures at sites d236 and SB_pk155 and minimizes air exchange with the surface from these cave sections.

Autumn ventilation

Although the autosampler and the atmospheric pressure and CO_2 readings from site SB_pk606 are limited to the winter – summer interval, leaving autumn dynamics open to inference, we can use available cave temperature and surface meteorological data to deduce the most likely scenario of autumn ventilation. In mid-September, surface temperature declines and sub-zero temperatures are established (day and night) by late-October or early November (Fig. 3). During this period, it is possible that ventilation is again enhanced at night when the cave is warmer than the surface – in the same fashion as in spring (Fig. 7c). This also marks the time when the soil becomes frozen, and infiltration of fresh precipitation ceases. Autumn precipitation also falls mainly as snow and blankets the cave (Fig. 2). The relatively warm (ca. +2°C) cave temperatures in mid-autumn at site d236 (Fig. 3) are stabilized by the snow cover that reduces ventilation and insulates the cave from the rapidly declining surface temperatures. Although westerly winds strengthen somewhat in September and October the winds decline by November when surface temperatures are considerably lower and the Siberian High intensifies to limit direct Westerlies airflow to Botovskaya Cave. The snowpack-induced blockage of the entrances and freezing in most joints impedes ventilation and results in a continued rise in cave air CO_2 due to continued infiltration through the yet unfrozen subsoil and epikarst until mid-September. Once the soil freezes, soil and epikarst water is trapped, and slower drip rates are likely to set in until late spring of the following year. The cave atmosphere is thus likely to shift into a near-stagnant phase, similar to the summer season, although the key mechanism is not the development of a cold trap but closure of the main venting points (entrances and joints).

Cave dripwater dynamics

Composition of autosampler-collected dripwater (Fig. 1) reveals a stable $\delta^{18}O$ signal of -17‰ across winter, spring, and summer, and suggests that infiltrating water is generally very well mixed (Fig. 5c). The observed dripwater $\delta^{18}O$ value is too negative to represent exclusively summer precipitation when infiltration is highest (Fig. 2) and likely includes some snowmelt component. The area above this section of the cave is influenced by both, isotopically very negative snow melt and isotopically less negative summer rainfall, which are then well mixed in the epikarst. Water infiltrates through overlying porous sandstone (matrix flow) and underlying fractured limestone (fracture flow). Both overlying sandstone and limestone likely consist of similarly fashioned fractures due to similar (Lower Ordovician) age and tectonic history, which means water of different ages and seasons can mix in the overburden and supress seasonal signals (Filippov, 2000).

Two outliers with higher $\delta^{18}O$ values (in April and July) seem to have suffered isotopic exchange with air (these vials contained little water possibly due to too low drip rates). A third outlier in August (the last sample) cannot be explained by isotopic exchange or kinetic isotope fractionation because this vial was full, without headspace. A possible explanation is that a warm season thunderstorm delivered a sufficient amount of rainfall with a less negative isotopic signature to push its isotope signal through the epikarst. Such a rain event might lead to higher fracture flow without much mixing with older waters. The sample ($\delta^{18}O$ signal of -16.58‰) was preceded by one high rainfall day in the week it was collected (August 18, 2022). However, given the small range of isotope values in the dripwater and the small number of dripwater samples, we caution that longer and more frequent sampling would be required for robust assessment of drip responses to individual infiltration events.

The linear relationship between cave water (dripwater and pond water) $\delta^{18}O$ and distance from the western cave entrances (Fig. 5b) requires explanation. Since all samples fall near the GMWL and LMWL this relationship cannot be explained by secondary evaporation. Although cave air relative humidity does vary (between ca. 80% in winter to near 100% in summer) in zone I and zone III, temperature remains stable at ca. +2°C, minimizing the evaporation potential. This notion is supported by the observation that pond water and dripwater $\delta^{18}O$ values are very similar. If evaporation significantly impacted these waters the isotopic signal of pond waters would be expected to be farther from the LMWL compared to dripwater, because the pond water is longer exposed to the cave atmosphere. We hypothesize that the observed eastward decline of cave water $\delta^{18}O$ reflects an increasing contribution of snow melt to the infiltrating waters in the deeper eastern section of the cave relative to the entrance (western) region. The western side of the cave is below a less vegetated slope, whereas the eastern section is below a gently undulating and forested plateau. The slope is more exposed to sunshine and allows for greater near-surface runoff of meltwater during spring snow melt, such that meltwater contributes very little to effective infiltration. Additionally, the less shaded western orientation with exposure to wind may support greater sublimation of snow, further reducing the opportunity for production of meltwater. The eastern surface is comparatively flat and covered in denser forest with deep mosses, which facilitates snow accumulation. Meltwater from the thick snowpack is more likely to infiltrate the underlying soil and a larger meltwater fraction would contribute to the dripwater budget, thereby lowering the dripwater $\delta^{18}O$ signature in the eastern cave sections.

Implications for speleothem growth and proxy dynamics

Temperature monitoring in the cave helps explain the speleothem deposition pattern in time and space. Speleothem deposition in the interglacials of the last ca. 700 ka (including the Holocene) is found only in easternmost zone III (Vaks et al. 2013, 2020). The present study shows that the modern average air temperature in zone I is +0.42 ± 0.6°C, in zone II +1.7 ± 0.07°C and in zone III +2.04 ± 0.04°C, i.e., zones I and II are much colder (and more variable) than zone III, the latter one more conducive to speleothem formation.

During the last decades Siberia warmed by at least ~3°C (Fedorov et al., 2024). This warming might also have led to an increase in cave air temperature, especially in zone I. Personal observations of expedition members testify to a significant reduction of the volume of ice in zone I compared to the early 2000s. This indicates that at times of lower-than-modern regional temperature, including many late-middle Quaternary interglacials, zones I and II might have been characterized by average sub-zero temperatures, which would have prevented speleothem formation in zones I and II. However, zone III was probably above 0°C during most interglacial periods over the last 700 kyrs, as reflected in the presence of speleothems there (Vaks et al., 2020; Margerum et al., 2025).

The monitoring results suggest that two main mechanisms control the $\delta^{18}O$ in speleothems in Botovskaya Cave. First, the observation that cave air temperature remains near constant at multi-annual scale and that the average $\delta^{18}O$ signal in dripwater and in precipitation overlap within error indicates that speleothem $\delta^{18}O$ is a reliable proxy for the $\delta^{18}O$ signal in precipitation. Cave air temperature will respond to long-term (centennial to millennial scale) changes in regional surface temperature, with a lag that results from inertia related to the warming of the surrounding host rock (Badino, 2004; Gabrovšek 2023). The dripwater composition will change together with regional precipitation patterns and the history of the incoming moisture.

Speleothems are likely to record changes in moisture source and precipitation seasonality which may alter this average value. The relationship between distance and $\delta^{18}O$ indicates that stalagmites from the eastern side of the cave would be fed by dripwater with a greater contribution of spring and autumn infiltration, compared to the western cave sections that receive a relatively higher fraction of summer infiltration. Dripwater and cave pond water in the deeper zone III retain an isotopic signal closer to the multi-annual average of precipitation. This suggests that isotope signals in stalagmites from the inner parts of Botovskaya Cave will replicate easier and reflect multi-annual changes in precipitation. The position of speleothems in the cave needs to be considered when interpreting speleothem $\delta^{18}O$ records. Given that dripwater $\delta^{18}O$ remains nearly constant at a given drip site and reflects the mean isotopic composition of precipitation (Fig. 5) stalagmites from Botovskaya Cave are likely to record decadal and longer-term changes in hydrological seasonality and moisture history.

Finally, the observed temperature and CO_2 dynamics suggest that horizontal Botovskaya Cave ventilates more actively in spring and (hypothetically) in autumn, whenever the cave air is warmer than the surface air and is not closed by ice and snow, while during winter ventilation driven by air density differences might be occasional.

CONCLUSIONS

The monitoring presented in this study highlights the complex interaction between temperature, precipitation, cave ventilation and dripwater isotopic composition in Botovskaya Cave in continental Eurasia. Multi-annual temperature, precipitation and cave water isotope, and CO_2 levels in Botovskaya Cave elucidate the mechanisms and parameters that influence the formation of speleothems in horizontal caves in near-permafrost regions. We find that ventilation dynamics vary seasonally, with different impacts on the cave temperature, depending on distance from the entrances. We have identified three thermal zones, of which zone III is the most stable, with a mean of +2.04 ± 0.04°C, in agreement with mean surface air temperature.

Cave ventilation is most active in spring, shortly after snowmelt when diurnal temperature changes at the surface and strong westerly winds invigorate air exchange with the cave. Ventilation is suppressed during summer when the cave acts as a cold air trap and reduced during wintertime when the cave entrances are covered with snow and when the ground is frozen so that (comparably) warm cave air can only slowly escape via large fractures near the entrances. The concentration of CO_2 in the cave air also varies seasonally, and on diurnal scale, which can be attributed to CO_2 production in soil and epikarst, infiltration and frost dynamics, and the variable impact of cave ventilation.

The assorted water isotope data from in and around Botovskaya Cave revealed that infiltrating waters correspond closely to the amount-weighted average composition of the precipitation above the cave. No significant secondary evaporation effects on the $\delta^{18}O$ signal are detected in the dripwater and cave pond water. A significant relationship between cave water $\delta^{18}O$ and distance from the entrance can be explained by season-specific infiltration pattern. A higher relative contribution of snowmelt water to the infiltrating waters in the eastern parts of the cave leads to lower dripwater $\delta^{18}O$ values, whereas the western cave sections receive more summer rainfall with less negative $\delta^{18}O$ signature. This indicates that speleothems from the western sections of the cave might comprise a slight bias towards the summer season, while stalagmites from the central and eastern cave reflect (multi-)annual mean precipitation.

These results provide important insights into the environmental processes that govern the microclimate in Botovskaya Cave and facilitate a more robust interpretation of future speleothem-based proxy reconstructions. Further, our work provides yet

another mechanism capable of explaining suboptimal reproducibility of stalagmite records from the same cave.

ACKNOWLEDGEMENTS

We would like to thank the Speleoclub Arabika members who facilitate and guide our research expeditions. We would also like to thank Julia Homann and Tobias Braun for their assistance and hard work during the 2022 research expedition to Botovskaya Cave. We thank Mohammadreza (Reza) Aghakashkooli for his tireless efforts in redesigning and improving our automatic drip logger, which provided vital information for this study. We would like to thank the residents of Konoshanovo village for their expansive local knowledge and abundant hospitality during our research visits. Finally, we would like to thank our reviewers for providing helpful comments and recommendations on the article. This research has been supported by the Leverhulme Trust who funded this research as part of the IsoPerm project (RPG-2020-334), and the Natural Environment Research Council (grant nos. NE/G013829/1 and NE/S007512/1).

Authorship statement: Study design: JM and SB. Field sampling and data acquisition: JM, SB, FAL, SU, AK, AO, DS, OG, AV, OK, and HM. Methodology/ Calculations: NM and JM. Original draft preparation: JM. Writing and editing: JM, SB, MB, SU, HM, NM, and OK.

REFERENCES

Allen, R.G., Pereira, L.S., Raes, D., Smith, M., 1998. Crop evapotranspiration: Guidelines for computing crop water requirements. FAO Irrigation and drainage, paper 56, Rome, 300 p.

Badino, G., 2004. Cave temperatures and global climatic change. International Journal of Speleology, 33(1), 103-113. http://dx.doi.org/10.5038/1827-806X.33.1.10

Baldini, J.U.L., Baldini, L.M., McDermott, F., Clipson, N., 2006. Carbon dioxide sources, sinks, and spatial variability in shallow temperate zone caves: evidence from Ballynamintra Cave, Ireland. Journal of Cave and Karst Studies, 68, 4–11.

Baldini, J.U.L., Lechleitner, F.A., Breitenbach, S.F.M., van Hunen, J., Baldini, L.M., Wynn, P.M., Jamieson, R.A., Ridley, H.E., Baker, A.J., Walczak, I.W., Fohlmeister, J., 2021. Detecting and quantifying palaeoseasonality in stalagmites using geochemical and modelling approaches. Quaternary Science Reviews, 254, 106784. https://doi.org/10.1016/j.quascirev.2020.106784

Box, M., Kononov, A., Serdyanjiv, N., Dashtseren, A., Sandag, K., Gutareva, O., Osintsev, A., Sokol'Nikov, D., Margerum, J., Kwiecien, O., Breitenbach, S.F.M., 2025. Seasonal temperature and ventilation changes govern proxy-signal transfer into caves in northern Mongolia. Cave and Karst Science, 51, 91–100.

Breitenbach, S.F.M., Lechleitner, F.A., Meyer, H., Diengdoh, G., Mattey, D., Marwan, N., 2015. Cave ventilation and rainfall signals in dripwater in a monsoonal setting – a monitoring study from NE India. Chemical Geology, 402, 111–124. https://doi.org/10.1016/j.chemgeo.2015.03.011

Cohen, J., Saito, K., Entekhabi, D., 2001. The role of the Siberian High in northern hemisphere climate variability. Geophysical Research Letters, 28, 299–302. https://doi.org/10.1029/2000GL011927

Columbu, A., Zhornyak, L.V., Zanchetta, G., Drysdale, R.N., Hellstrom, J.C., Isola, I., Regattieri, E., Fallick, A.E., 2023. A mid-Holocene stalagmite multiproxy record from southern Siberia (Krasnoyarsk, Russia) linked to the Siberian High patterns. Quaternary Science Reviews, 320, 108355. https://doi.org/10.1016/j.quascirev.2023.108355

Craig, H., 1961. Isotopic variations in meteoric waters. Science, 133, 1702–1703.

Cui, Z., Wu, G.-L., Huang, Z., Liu, Y., 2019. Fine roots determine soil infiltration potential than soil water content in semi-arid grassland soils. Journal of Hydrology, 578, 124023. https://doi.org/10.1016/j.jhydrol.2019.124023

Dsouza, K.B., Ofosu, E., Boudreault, R., Moreno-Cruz, J., Leonenko, Y., 2025. Substantial carbon removal capacity of Taiga reforestation and afforestation at Canada's boreal edge. Communications Earth & Environment, 6, 893. https://doi.org/10.1038/s43247-025-02822-z

Ekaykin, A.A., 2016. Stable isotopes of water in glaciology and paleogeography. Methodological manual. State Research Centre of the Russian Federation Arctic and Antarctic Research Institute, Saint Petersburg, 69 p. [In Russian].

Fairchild, I.J., Baker, A., 2012. Speleothem science: From process to past environments, Wiley, Oxford, 448 p.

Fang, Y., Du, X., Ye, X., Wang, E., 2024. Groundwater response to snowmelt infiltration in seasonal frozen soil areas: site monitoring and numerical simulation. Hydrology, 11, 201. https://doi.org/10.3390/hydrology11120201

Fedorov, A.N., Konstantinov, P.Y., Vasilyev, N.F., Varlamov, S.P., Skachkov, Y.B., Gorokhov, A.N., Kalinicheva, S.V., Ivanova, R.N., Petrova, A.N., Andreeva, V.V., Novopriezzhaya, V.A., Sivtsev, M.A., Zheleznyak, M.N., 2024. Climate and permafrost shifts in Yakutia's Arctic and Subarctic from 1965 to 2023. Land, 13, 2150.

Filippov A.G., 2000. Speleogenesis of the Botovskaya Cave, Eastern Siberia. In: Klimchouk, A.B., Ford, D.C., Palmer, A.N., Dreybrodt, W. (Eds.), Speleogenesis. Evolution of karst aquifers. National Speleological Society, Huntsville, p. 282–286.

Frisia, S., 2019. Stalactites and stalagmites. In: White, W.B., Culver, D.C., Pipan, T. (Eds.), Encyclopedia of caves (3rd Ed.). Academic Press, London, p. 1041–1048. https://doi.org/10.1016/B978-0-12-814124-3.00120-5

Haude, W., 1955. Zur Bestimmung der Verdunstung auf möglichst einfache Weise. Mitteilungen Deutscher Wetterdienst, 11, 1–24.

Gabrovšek, F., 2023. How do caves breathe: The airflow patterns in karst underground. PLOS ONE, 18, e0283767. https://doi.org/10.1371/journal.pone.0283767

Gao, T., Song, X., Ren, Y., Liu, H., Meng, Y., Dong, X., 2023. Effects of seasonal changes on the carbon dynamics in mixed coniferous forests. PLOS ONE, 18, e0267365. https://doi.org/10.1371/journal.pone.0267365

Golubtsov, V.A., Cherkashina, A.A., Vanteeva, Yu.V., Voropay, N.N., Turchinskaya, S.M., 2023. Variations in the stable carbon isotopic composition of soil organic matter in mountain depressions of the Cis-Baikal

region. Contemporary Problems of Ecology, 16, 776–789. https://doi.org/10.1134/S1995425523060094

James, E.W., Banner, J.L., Hardt, B., 2015. A global model for cave ventilation and seasonal bias in speleothem paleoclimate records. Geochemistry, Geophysics, Geosystems, 16, 1044–1051. https://doi.org/10.1002/2014GC005658

Juhls, B., Stedmon, C.A., Morgenstern, A., Meyer, H., Hölemann, J., Heim, B., Povazhnyi, V., Overduin, P.P., 2020. Identifying drivers of seasonality in Lena River biogeochemistry and dissolved organic matter fluxes. Frontiers in Environmental Science, 8, 53. https://doi.org/10.3389/fenvs.2020.00053

Kostrova, S.S., Meyer, H., Fernandoy, F., Werner, M., Tarasov, P.E., 2020. Moisture origin and stable isotope characteristics of precipitation in southeast Siberia. Hydrological Processes, 34, 51–67. https://doi.org/10.1002/hyp.13571

Kukuljan, L., Gabrovšek, F., Covington, M.D., Johnston, V.E., 2021. CO_2 dynamics and heterogeneity in a cave atmosphere: role of ventilation patterns and airflow pathways. Theoretical and Applied Climatology, 146, 91–109. https://doi.org/10.1007/s00704-021-03722-w

Lechleitner, F.A., Mason, A.J., Breitenbach, S.F.M., Vaks, A., Haghipour, N., Henderson, G.M., 2020. Permafrost-related hiatuses in stalagmites: Evaluating the potential for reconstruction of carbon cycle dynamics. Quaternary Geochronology, 56, 101037. https://doi.org/10.1016/j.quageo.2019.101037

Margerum, J., Homann, J., Umbo, S., Nehrke, G., Hoffmann, T., Vaks, A., Kononov, A., Osintsev, A., Giesche, A., Mason, A., Lechleitner, F.A., Henderson, G.M., Kwiecien, O., Breitenbach, S.F.M., 2025. Reconstruction of Holocene and Last Interglacial vegetation dynamics and wildfire activity in southern Siberia. Climate of the Past, 21, 661–677. https://doi.org/10.5194/cp-21-661-2025

Menne, M.J., Durre, I., Vose, R.S., Gleason, B.E., Houston, T.G., 2012. An overview of the global historical climatology network-daily database. Journal of Atmospheric and Oceanic Technology, 29, 897-910. https://doi.org/10.1175/JTECH-D-11-00103.1 [accessed: August 3, 2025].

Meyer, H., Schönicke, L., Wand, U., Hubberten, H.W., Friedrichsen, H., 2000. Isotope studies of hydrogen and oxygen in ground ice-experiences with the equilibration technique. Isotopes in Environmental and Health Studies, 36, 133–149. https://doi.org/10.1080/10256010008032939

Muñoz Sabater, J., 2019. ERA5-Land hourly data from 1950 to present. Copernicus Climate Change Service (C3S) Climate Data Store (CDS). [accessed: October 17, 2025] https://doi.org/10.24381/cds.e2161bac

Obu, J., Westermann, S., Bartsch, A., Berdnikov, N., Christiansen, H.H., Dashtseren, A., Delaloye, R., Elberling, B., Etzelmüller, B., Kholodov, A., Khomutov, A., Kääb, A., Leibman, M.O., Lewkowicz, A.G., Panda, S.K., Romanovsky, V., Way, R.G., Westergaard-Nielsen, A., Wu, T., Yamkhin, J., Zou, D., 2019. Northern Hemisphere permafrost map based on TTOP modelling for 2000–2016 at 1 km^2 scale. Earth-Science Reviews, 193, 299–316. https://doi.org/10.1016/j.earscirev.2019.04.023

Pacton, M., Breitenbach, S.F.M., Lechleitner, F.A., Vaks, A., Rollion-Bard, C., Gutareva, O.S., Osintcev, A.V., Vasconcelos, C., 2013. The role of microorganisms in the formation of a stalactite in Botovskaya Cave, Siberia – paleoenvironmental implications. Biogeosciences, 10, 6115–6130. https://doi.org/10.5194/bg-10-6115-2013

Peel, M.C., Finlayson, B.L., McMahon, T.A., 2007. Updated world map of the Köppen-Geiger climate classification. Hydrology and Earth System Sciences,11, 1633–1644. https://doi.org/10.5194/hess-11-1633-2007

Perşoiu, A., Ionita, M., Weiss, H., 2019. Atmospheric blocking induced by the strengthened Siberian High led to drying in west Asia during the 4.2 ka BP event – a hypothesis. Climate of the Past, 15, 781–793. https://doi.org/10.5194/cp-15-781-2019

Pla, C., Cuezva, S., Garcia-Anton, E., Fernandez-Cortes, A., Cañaveras, J.C., Sanchez-Moral, S., Benavente, D., 2016. Changes in the CO_2 dynamics in near-surface cavities under a future warming scenario: Factors and evidence from the field and experimental findings. Science of The Total Environment, 565, 1151–1164. https://doi.org/10.1016/j.scitotenv.2016.05.160

Ponomarev, E., I., Kharuk, V.I., Ranson, K.J., 2016. Wildfires dynamics in Siberian larch forests. Forests, 7, 125. https://doi.org/10.3390/f7060125

Rau, G.C., Cuthbert, M.O., Andersen, M.S., Baker, A., Rutlidge, H., Markowska, M., Roshan, H., Marjo, C.E., Graham, P.W., Acworth, R.I., 2015. Controls on cave drip water temperature and implications for speleothem-based paleoclimate reconstructions. Quaternary Science Reviews, 127, 19–36. https://doi.org/10.1016/j.quascirev.2015.03.026

Ridley, H., Baldini, J., Prufer, K., Walczak, I., Breitenbach, S., 2015. High-resolution monitoring of Yok Balum Cave, Belize: An investigation of seasonal ventilation regimes and the atmospheric and drip-flow response to a local earthquake. Journal of Cave and Karst Studies, 77, 183–199. https://doi.org/10.4311/2014ES0117

Riechelmann, S., Breitenbach, S., Schroder-Ritzrau, A., Mangini, A., Immenhauser, A., 2019. Ventilation and cave air PCO_2 in the Bunker-Emst Cave System (NW Germany): implications for speleothem proxy data, Journal of Cave and Karst Studies, 81, 98–112. https://doi.org/10.4311/2018ES0110

Sawamoto, T., Hatano, R., Yajima, T., Takahashi, K., Isaev, A.P., 2000. Soil respiration in Siberian Taiga ecosystems with different histories of forest fire. Soil Science and Plant Nutrition, 46, 31–42. https://doi.org/10.1080/00380768.2000.10408759

Schiedung, M., Bellè, S.-L., Malhotra, A., Abiven, S., 2022. Organic carbon stocks, quality and prediction in permafrost-affected forest soils in North Canada. Catena, 213, 106194. https://doi.org/10.1016/j.catena.2022.106194

Smerdon, J.E., Pollack, H.N., Cermak, V., Enz, J.W., Kresl, M., Safanda, J., Wehmiller, J.F., 2004. Air-ground temperature coupling and subsurface propagation of annual temperature signals. Journal of Geophysical Research: Atmospheres, 109, D21107. https://doi.org/10.1029/2004JD005056

Smerdon, J.E., Pollack, H.N., Enz, J.W., Lewis, M.J., 2003. Conduction-dominated heat transport of the annual temperature signal in soil. Journal of Geophysical Research: Solid Earth, 108(B9), 2431. https://doi.org/10.1029/2002JB002351

Vaks, A., Gutareva, O.S., Breitenbach, S.F.M., Avirmed, E., Mason, A.J., Thomas, A.L., Osinzev, A.V., Kononov, A.M., Henderson, G.M., 2013. Speleothems reveal 500,000-year history of Siberian permafrost. Science, 340, 183–186. https://doi.org/10.1126/science.1228729

Vaks, A., Mason, A., Breitenbach, S.F.M., Giesche, A., Osinzev, A., Adrian, I., Kononov, A., Umbo, S.,

Lechleitner, F.A., Rosensaft, M., Henderson, G.M., 2025. Arctic speleothems reveal nearly permafrost-free Northern Hemisphere in the late Miocene. Nature Communications, 16, 5483. https://doi.org/10.1038/s41467-025-60381-5

Vaks, A., Mason, A.J., Breitenbach, S.F.M., Kononov, A.M., Osinzev, A.V., Rosensaft, M., Borshevsky, A., Gutareva, O.S., Henderson, G.M., 2020. Palaeoclimate evidence of vulnerable permafrost during times of low sea ice. Nature, 577, 221–225. https://doi.org/10.1038/s41586-019-1880-1

Wang, J., Guan, Y., Wu, L., Guan, X., Cai, W., Huang, J., Dong, W., Zhang, B., 2021. Changing Lengths of the Four Seasons by Global Warming. Geophysical Research Letters, 48, e2020GL091753. https://doi.org/10.1029/2020GL091753

Wong, C.I., Breecker, D.O., 2015. Advancements in the use of speleothems as climate archives. Quaternary Science Reviews, 127, 1–18. https://doi.org/10.1016/j.quascirev.2015.07.019